466 *Biochemistry* **2011,** *50,* 466–479
DOI: 10.1021/bi1009634

BIOCHEMISTRY
including biophysical chemistry & molecular biology
Article

Membrane Insertion Topology of the Central Apolipoprotein A-I Region. Fluorescence Studies Using Single Tryptophan Mutants[†]

Eduardo D. Prieto and Horacio A. Garda*

Instituto de Investigaciones Bioquímicas de La Plata (INIBIOLP), Consejo Nacional de Investigaciones Científicas y Técnicas (CONICET), Universidad Nacional de La Plata (UNLP), Facultad de Ciencias Médicas, Calles 60 y 120, 1900-La Plata, Argentina

Received June 14, 2010; Revised Manuscript Received December 7, 2010

ABSTRACT: Apolipoprotein A-I (apoAI) contains several amphipathic α-helices. To carry out its function, it exchanges between lipid-free and different lipidated states as bound to membranes or to lipoprotein complexes of different morphology, size, and composition. When bound to membranes or to spherical lipoprotein surfaces, it is thought that most α-helices arrange with their long axis parallel to the membrane surface. However, we previously found that a central region spanning residues 87−112 is exclusively labeled by photoactivable reagents deeply located into the membrane (Córsico et al. (2001) *J. Biol. Chem. 276*, 16978−16985). A pair of amphipathic α-helical repeats with a particular charge distribution is predicted in this region. In order to study their insertion topology, three single tryptophan mutants, each one containing the tryptophan residue at a selected position in the hydrophobic face of the central Y-helices (W@93, W@104, and W@108), were used. From the accessibility to quenchers located at different membrane depths, distances from the bilayer center of 13.4, 10.5, and 15.7 Å were estimated for positions 93, 104, and 108, respectively. Reported data also indicate that distances between homologous positions (in particular for W@93 and W@104) are very short in dimers in aqueous solution, but they are larger in membrane-bound dimers. Data indicate that an intermolecular central Y-helix bundle would penetrate the membrane perpendicularly to the membrane surface. Intermolecular helix−helix interactions would occur through the hydrophilic helix faces in the membrane-bound bundle but through the hydrophobic faces in the case of dimers in solution.

Apolipoprotein A-I (apoAI)[1] is the major protein of high-density lipoproteins (HDL) which plays a key role in the reverse cholesterol transport pathway that delivers excess of cholesterol back to the liver for clearance (*1*). Like other exchangeable apolipoproteins, apoAI behaves as an amphitropic protein. To carry out its function, apoAI cycles among a lipid-free or lipid-poor form, a membrane-bound state, and bound to discoidal or spherical HDL of different size and composition (*2*).

The basic common structural motif shared by exchangeable apolipoproteins is the amphipathic α-helix (*3*). Mature human ApoAI contains 243 amino acid residues, and computational analysis reveals the presence at the N-terminus of a G* amphipathic α-helix, which is similar to those found in globular proteins. The region of residues 44−243, encoded by exon 4, is composed of 10 repeats predicted to form amphipathic α-helices mostly punctuated by proline residues. Six of these repeats are 22mer class A α-helices, which are typical in all exchangeable apolipoproteins and characterized by positive charge clusters at the hydrophilic/hydrophobic helix interface and negative residue clusters at the polar face center. There are also two pairs of amphipathic α-helical repeats (3−4 and 9−10) differing in the polar face charge distribution. Each of them contains a short 11mer repeat (3 or 9) separated by proline from a 22mer repeat (4 or 10). These repeats are called class Y α-helices because the distribution of three positively charged residues resembles a Y letter, with the hydrophobic face between the arms, and two negatively charged clusters between arms and the base of the Y.

A crystal structure of an apoAI fragment with the N-terminal G* helix deleted (Δ1−43 apoAI) was obtained (*4*). It shows a horseshoe-shaped tetramer with the monomers extended and highly helicoidal, which is thought to be related with the lipid-bound state. Evidence obtained by other techniques does not totally agree with this structure, but it coincides in the following views: (a) in the lipid-free state, the helical repeats fold in bundles of relatively loose tertiary structure stabilized by contacts among the α-helix nonpolar faces (*5*), and (b) helical bundles should be opened in order to expose most of the helix nonpolar faces for binding lipids (*6*).

ApoAI reacts with phospholipid vesicles at the gel to liquid-crystalline phase transition temperature range, for example, with dimyristoylphosphatidylcholine (DMPC) vesicles near 24 °C, generating micellar lipoprotein complexes of discoidal morphology (*7*). However, apoAI binds to bilayers of zwitterionic phospholipids at the liquid-crystalline or liquid-ordered states, for example, with 1-palmitoyl-2-oleoylphosphatidylcholine (POPC) or POPC/cholesterol vesicles, without vesicle disruption (*8*, *9*). It was proposed that amphipathic class A amphipathic α-helices bind to phospholipid surfaces according to the snorkel model (*10*), embedding the hydrophobic face within the lipids while

[†]This work was supported by grants from Consejo Nacional de Investigaciones Científicas y Técnicas (CONICET), Agencia Nacional de Promoción Científica y Tecnológica, and Universidad Nacional de La Plata to H.A.G. E.D.P. is a postdoctoral fellow, and H.A.G. is a member of the scientific research career from CONICET, Argentina.

*To whom correspondence should be addressed. E-mail: hagarda@isis.unlp.edu.ar. Phone: 54-221-4824894. Fax: 54-221-4258988.

[1]Abbreviations: apoAI, apolipoprotein A-I; HDL, high-density lipoproteins; DMPC, dimyristoylphosphatidylcholine; POPC, 1-palmitoyl-2-oleoylphosphatidylcholine; W, tryptophan; *n*-doxyl-PC, *n*-doxylphosphatidylcholine; tempo-PC, tempo-phosphatidylcholine.

 Published on Web 12/08/2010

positive residues interact electrostatically with negative phosphate groups of membrane phospholipids. It is not known, however, if the particular charge distribution of class Y helices plays some role in the lipid binding process. Since these type Y helical repeats are unique in apoAI, and in particular the repeat pair 3−4 has been proposed to be responsible for several functional properties of this protein (*11*−*14*), it is of particular interest to obtain information about its conformation and conformational adaptability in the lipid binding process.

We have previously shown by using a photoactivable radiolabeled phospholipid analogue (^{125}I-TID/PC) incorporated into POPC or POPC/cholesterol vesicles that only the apoAI region spanning residues 87−112 becomes labeled when the protein is mixed with ^{125}I-TID/PC loaded vesicles (*11*). This fact indicates that when apoAI is bound to phospholipid vesicles, at least some amino acid residues within the central class Y helix pair 3−4 would penetrate the lipid bilayer deeply enough to be reached by the reactive diazirine group which is located near the center of the lipid bilayer, while the rest of the lipid interacting amphipathic α-helices would be more superficially located. Among others, two possibilities can explain this fact: (a) The central type Y α-helices are inserted into the membrane bilayer with their long axis parallel to the phospholipid hydrocarbon chains. (b) These α-helical repeats interact with the membrane according to the snorkel model with the long helix axis parallel to the surface but embedding the nonpolar faces into the lipid bilayer more deeply than the other apoAI helical repeats.

The aim of this work was to obtain information about the mechanism and topology of membrane insertion of this apoAI region trying to distinguish between the above-mentioned possibilities. A set of three single tryptophan mutants (W@93, W@104, and W@108), each one containing the tryptophan (W) residue at a selected position in the hydrophobic face of the central Y-helix pair, was used. Accessibility to paramagnetic quenchers located at different membrane depths, 1-palmitoyl-2-stearoyl-(*n*-doxyl)-*sn*-glycero-3-phosphocholine where n = 5, 10, or 14 (*n*-doxyl-PC), and 1-palmitoyl-2-oleoyl-*sn*-glycero-3-phospho(tempo)choline (tempo-PC), allowed to estimate the membrane insertion depth for each position reported by W residues in the mutants. The results indicated that the 3−4 class Y helix pair inserts into the lipid bilayer with its long helix axis almost perpendicular to the lipid surface.

EXPERIMENTAL PROCEDURES

Materials. DMPC, POPC, and cholesterol were purchased from Avanti Polar Lipids (Alabaster, AL). Spin-labeled lipids were from Molecular Probes (Eugene, OR). All other reagents were of analytical grade.

ApoAI Single Tryptophan Mutants. The mutants W@93, W@104, and W@108 were obtained by site-directed mutagenesis starting from the cDNA of a mutant containing no W in its sequence (W@0). The cDNA of W@0 inserted in a pET-30 plasmid (Novagen, Madison, WI) was kindly donated by S. Davidson (University of Cincinnati, OH). In this construction, the four naturally occurring W residues (positions 8, 50, 72, and 108) were replaced by phenylalanine (*15*). Besides, this construction contained an IgA protease cleavage site between the pro-segment and the beginning of the mature apoAI gene (*16*). Cleavage with IgA protease leaves two extra amino acids (Thr-Pro) at the N-terminal, which have no consequence on the apoAI structural or functional properties (*16*). Site-directed mutagenesis was carried out as previously described (*17*) using the commercial kit QuickChange, manufactured by Stratagene. Primer design and PCR reactions were performed according to the manufacturer's instructions using *Pfu-Turbo* DNA polymerase. After digestion of the template with *Dpn*I, competent JM109 cells were transformed. The plasmid DNA of the transformed bacteria was sequenced from the S-tag and T7-terminator sites. The service of Macrogen Inc. (Seoul, Korea) was used for primer synthesis and DNA sequencing. BL21 (DE3) expression host cells were transformed with the plasmids containing the correct sequences. After induction with isopropyl 1-thio-β-D-galactopyranoside, the His-tagged fusion proteins were extracted with 3 M guanidine hydrochloride and purified by immobilized metal affinity chromatography on Ni columns (GE Healthcare Bio-Sciences AB, Uppsala, Sweden). The fusion proteins were cleaved with IgA protease (MoBiTec, Göttingen, Germany) at a mass to mass concentration of 1:2000 (enzyme:protein) for 24 h at 32 °C in 20 mM Tris-HCl and 5 mM EDTA, pH 7.8. A second metal affinity chromatography step was used to separate the final mutants from contaminant free His-tag and uncleaved protein. SDS−PAGE on 12% gels was used to check each step during expression and purification. To confirm identity, mutant protein preparations were also checked by MALDI-TOF analysis in a Bruker Ultraflex II mass spectrometer (Service of the "Centro de Estudios Químicos y Biológicos por Espectrometría MALDI-TOF", Departamento de Química Biológica, Facultad de Ciencias Exactas, Universidad de Buenos Aires, Buenos Aires, Argentina).

Circular Dichroism. Far-UV CD spectra of the mutants at a concentration of 0.1 g/L were acquired at 25 °C in a Jasco CD spectrophotometer, Model 715 (Service of the Departamento de Ciencia y Tecnología, Universidad Nacional de Quilmes, Bernal, Buenos Aires, Argentina). Spectra were corrected using the buffer as blank.

DMPC Liposome Clearance. DMPC in chloroform was dried down with flushing N_2 in a glass tube leaving a thin lipid layer. After 2 h in vacuum, lipids were brought up in 25 mM sodium phosphate buffer at a concentration of 10 mM. Multilamellar liposomes were made by extensive vortexing at 35 °C. They were mixed with the proteins at the phase transition temperature of DMPC (24 °C) at a molar ratio of 40/1 (final protein concentration of 0.2 g/L), and the decrease in light scattering with time was analyzed by following the optical density at 350 nm. The product of the reaction was analyzed by native gradient polyacrylamide gel electrophoresis in 4−20% gels.

Preparation of Unilamellar POPC/Cholesterol Vesicles with or without Spin-Labeled Lipid Analogues. Vesicles were prepared containing the following: POPC/cholesterol (4/1 in molar ratio); POPC/spin-labeled phospholipid/cholesterol (3/1/1 molar ratio) where the spin-labeled phospholipids were 5-, 10-, or 14-doxyl-PC or tempo-PC (labeled in the polar choline group); POPC/3-β-doxylcholestane (4/1 molar ratio). For this, the appropriate lipid mixtures in chloroform were dried and resuspended in aqueous buffer as above mentioned for DMPC. Then, liposomes were treated for 10 min with ultrasound and extruded by ten passages through polycarbonate filters (100 nm pore) using a LiposoFast extruder (Avestin Inc., Otawa, Canada).

Fluorescence Spectroscopy Measurements. Tryptophan fluorescence emission spectra were obtained in an Olis upgraded SLM4800 spectrophotofluorometer (Olis Inc., Bogart, GA) in cells of 0.2 cm path length for excitation and 1 cm for emission. Excitation wavelength was 295 nm, and emission was scanned from 300 to 550 nm. A resolution of 8 nm bandwidth was used for both excitation and emission. The mutant containing no W was used for

background subtraction. Spectra in the presence of lipid vesicles (containing or not spin-labeled lipids) were corrected by inner filter effect according to $F(\lambda)corr = F(\lambda)\ 10^{[0.1OD295+0.5OD(\lambda)]}$, where $F(\lambda)$corr and $F(\lambda)$ are the corrected and uncorrected spectra, respectively, OD295 is the optical density of the sample at 295 nm, and OD(λ) is the absorption spectra of the sample between 300 and 550 nm. Glan Thompson polarizers were used for anisotropy measurements. In this case, excitation wavelength was 295 nm (8 nm bandwidth), and emission was set at 340 nm (16 nm bandwidth). All of the measurements were made in triplicate, and the average value is given.

Fluorescence Homoquenching and Energy Homotransfer in Lipid-Free ApoAI Oligomers. Models Used for Estimation of Intermolecular Distances between Homologous Residues. Several models for the self-association equilibrium of apoAI in aqueous solutions, as well as for the dependence of the fluorescence homoquenching and energy homotransfer on the oligomer size, were considered in order to estimate the average intermolecular distances between homologous W residues in the aggregates from the variation of the fluorescence intensity and anisotropy with the protein concentration.

(*a*) *Models Considered for ApoAI Self-Association Equilibrium.* Any model for oligomerization equilibrium should fulfill the relationship:

$$[Pt] = \sum_{n=1}^{m}[Pn] = \sum_{n=1}^{m} Kn[P]^n \quad (1)$$

where m is the maximal oligomer size; [Pt], [Pn], and [P] are respectively the total protein concentration, the concentrations of each one of the n-sized oligomers, and the concentration of the monomeric protein in weight/volume units; while Kn is the equilibrium constant for each oligomerization step. Some oligomerization steps can be absent. For example, in a monomer−dimer−tetramer−octamer equilibrium, K3 = K5 = K6 = K7 = 0 and

$$[Pt] = [P] + K2[P]^2 + K4[P]^4 + K8[P]^8 \quad (2)$$

Kn for each step are frequently interrelated in a way that

$$[Pt] = \sum_{n=1}^{m} f(n)K^{n-1}[P]^n \text{ (for sequential monomer addition)} \quad (3)$$

or

$$[Pt] = [P] + \sum_{n=1}^{m} f(n)K^{2n-1}[P]^{2n} \text{ (for sequential dimer addition)} \quad (4)$$

where K is the equilibrium constant for the first step (or dimerization) and f(n) is a particular function of n depending on the particular oligomerization mechanism and stoichiometric considerations. Frequently, f(n) = 1 or f(n) = n.

A particular simplification of eq 3 is obtained if m = ∞ and K[P] < 1. In this case, the series is convergent, and [P] and [Pt] will be related by

$$[P] = [Pt]/(1 + K[Pt]) \text{ if } f(n) = 1 \quad (5)$$

or

$$[P] = (2K[Pt] + 1 - \text{sqrt}(4K[Pt] + 1))/(2K^2[Pt]) \text{ if } f(n) = n \quad (6)$$

(*b*) *Models Considered for W Fluorescence Homoquenching in ApoAI Oligomers.* The fluorescence intensity normalized to the total protein concentration will be

$$FN = Ft/[Pt] = \sum_{n=1}^{m}\frac{sFn[Pn]}{[Pt]} = \sum_{n=1}^{m}\frac{sFn\ Kn[P]^n}{[Pt]}$$

$$= \sum_{n=1}^{m}\frac{sFn\ f(n)K^{n-1}[P]^n}{[Pt]} \quad (7)$$

where Ft is the total fluorescence of the sample and sFn is the specific fluorescence intensity (per unit of concentration) for the oligomer of size n.

A pure energy homotransfer process does not affect the quantum yield, and in this case sFn should be equivalent to the specific fluorescence of the monomer (sF1). As shown in the Results section, however, it is not the case for the single W mutants used here, and some process resulting in homoquenching of the fluorescence emission in the oligomers is present. If W residues in oligomers are equidistant and interacting equally, the rate of the process conducing to homoquenching can be assumed to be proportional to n − 1 (i.e., the number or the fraction of other fluorophores that can quench the emission of each fluorescent group in the oligomer). Thus

$$sFn = sF1/(1 + (n-1)Khq) \quad (8)$$

where Khq is the rate constant for the homoquenching process.

Another possibility is that the homoquenching process in oligomers is due only to the interaction between pairs of W residues close together but far away from other W (or W pairs). For example, in the considered monomer−dimer−tetramer−octamer model, two dimers suffering homoquenching could be arranged in larger oligomers (tetramers or octamers) without further change in the homoquenching efficiency. In this case

$$sFn = sF1 \text{ for } n = 1 \text{ and}$$
$$sFn = sF1/(1 + Khq) \text{ for } n \geq 2 \quad (9)$$

(*c*) *Models Considered for W Fluorescence Homotransfer in ApoAI Oligomers.* The dependence of the fluorescence anisotropy on the energy homotransfer in different sized oligomers has been well described by Runnels and Scarlatta (*18*). If considering that all fluorophores in the oligomer are equidistantly separated by a distance (R) independently of the oligomer size, as well as the average emission anisotropy following homotransfer is equal to zero, the anisotropy of the fluorescence arising from an oligomer of size n (rn) is given by the following equation if depolarizing rotation is absent:

$$rn = r1\frac{1 + (R0/R)^6}{1 + n(R0/R)^6} \quad (10)$$

where r1 is the fluorescence anisotropy of free monomer and R0 is Foster's distance. In the presence of depolarizing rotation, rn is given by the following more complex equation, where r0 is the fundamental anisotropy:

$$rn = \frac{r1r0(1+(R0/R)^6)^2}{r0 + (r1(n-1) + 2r0)(R0/R)^6 + nr0(R0/R)^{12}} \quad (11)$$

As shown by Runnels and Scarlatta, however, the influence of depolarizing rotation is not noticeable when R < 0.8 R0, and in this case the simplest eq 10 gives essentially the same results.

As considered above for homoquenching, if homotransfer in higher oligomers occurs only between pairs of W residues far

away from other W, the efficiency of this process can become independent of the oligomer size if n ≥ 2. Thus, in this case

$$rn = r1 \text{ for } n = 1 \text{ and}$$

$$rn = r1(1+(R0/R)^6)/(1+2(R0/R)^6) \text{ for } n \geq 2 \quad (12)$$

Because of the anisotropy additive properties, in a mixture of different sized oligomers at equilibrium, the resultant anisotropy (r) will be

$$r = \sum_{n=1}^{m} \frac{rn\ sFn[Pn]}{Ft} = \sum_{n=1}^{m} \frac{rn\ sFn\ Kn[P]^n}{Ft} \text{ or}$$

$$r = \sum_{n=1}^{m} \frac{rn\ sFn\ f(n)K^{n-1}[P]^n}{Ft} \quad (13)$$

where Ft = ∑sFn[Pn] is the total fluorescence intensity of the mixture.

Nonlinear Regression Fittings Used To Calculate Intermolecular Distances in Oligomers. The regression wizard of SigmaPlot 8.0 software was used with this aim. Global fits to the experimental data of the three mutants were made assuming the same oligomerization equilibra (i.e., the same K values) for all of the mutants. In a linked system, the general eqs 4 and 9 were fitted to the experimentally obtained data of FN and r, respectively. These general equations were used with different assumptions for m and f(n), as well as the different mentioned alternatives for sFN or rn. For m between 2 and 4, [P] values for each one of the used [Pt] were given by the exact solutions with physical meaning of the corresponding quadratic, cubic, and quartic polynomials arising from eq 3. As a general solution with any m value, eq 3 was also included in the linked equation system to be fitted to the experimentally used [Pt] values in order to calculate the corresponding values for [P]. A higher weight was used in fittings to [Pt] in comparison to r and FN, thus assuring that eq 3 is exactly satisfied. When applied for m = 2, 3, or 4, this approach gave essentially the same results as the above-described exact solutions for [P], indicating its general applicability. In this way, the values of sF1, r1, Khq, and R were individually calculated for each one of the mutants, while a unique value for K was calculated assuming that it is the same for the three mutants. When the model of monomer−dimer−tetramer−octamer equilibrium was assumed, the values for K2, K4, and K8 obtained by Vitello and Scanu (*19*) from sedimentation equilibrium ultracentrifugation were used as fixed parameters or were supposed to be related in the same way as in eq 3 (i.e., $Kn = f(n)K^{n-1}$).

The sum of the squares of the residuals and visual inspection of the predicted values for the fitted functions were used as a parameter of the fit goodness.

Foster's Distance (R0) Estimations. R0 values for each mutant were estimated using the relationship (*20*):

$$R0 = 0.211(\kappa^2 n^{-4} Q J(\lambda))^{1/6} \quad (14)$$

where the orientation factor (κ^2) and the refractive index of the medium (n) were assumed to be 0.67 and 1.4, respectively (*20*). The quantum yields Q were obtained individually for each mutant from the extrapolated values of specific fluorescence intensities obtained by the fittings, relative to the emission intensity obtained for a reference solution of tryptophan in water for which Q was assumed as 0.13 (*21*). The spectral overlap integral, $J(\lambda)$ (in units of $M^{-1}\ cm^{-1}\ nm^4$) was also calculated for each mutant from their absorption and normalized fluorescence spectra. In this way, R0 values of 10.41, 10.18, and 11.05 Å were estimated for the W of W@93, W@104, and W@108, respectively.

Binding of ApoAI Mutants to Lipid Vesicles. Tryptophan emission spectra of W@93, W@104, and W@108 were measured in the presence of increasing concentrations of POPC/cholesterol (4/1 molar ratio) unilamellar vesicles containing or not spin-labeled lipids. After background subtraction and correction by inner filter, fluorescence intensity was obtained by spectral integration. ApoAI binding to lipid vesicles has been previously shown to follow a simple equilibrium (*8*) described by

$$[Pb] = (1/2)\{(Kd + N[Vt] + [Pt]) - sqrt((Kd+N[Vt]+[Pt])^2 - 4N[Vt][Pt])\} \quad (15)$$

where [Pb] is the concentration of bound protein, [Pt] is the total protein concentration in the sample, [Vt] is the total vesicle concentration in the sample expressed in concentration of POPC, N is the upper limit of [Pb]/[Vt] or the number of vesicle sites available for binding when [Vt] = 1, and Kd is the dissociation equilibrium constant.

On the other hand, the total fluorescence intensities of the proteins in the presence of vesicles (Fv) are given by the sum of the fluorescence intensities of bound (Fb) and unbound (Fub) protein: Fv = Fb + Fub. The emission intensity of bound protein (Fb) is the product of its concentration ([Pb]) by its specific fluorescence intensity (sFb): Fb = [Pb]sFb. If oligomerization of unbound protein is not considered, its emission intensity (Fub) will be simply its concentration ([Pub] = [Pt] − [Pb]) multiplied by its specific fluorescence intensity (sFub). As shown in the Results section, however, the fluorescence intensity of the free protein in solution (or unbound protein) is considerably affected by their oligomerization especially in W@93 and W@104. Oligomerization equilibrium of the unbound protein should be displaced toward a higher proportion of monomers (having a higher quantum yield than oligomers) when the concentration of lipid vesicles increases and consequently the concentration of unbound protein decreases. In order to take this fact into account, the fluorescence intensity of the unbound protein (Fub) can be expressed by a function fitting well to the fluorescence intensity dependence on the free protein concentration (see Figure 1), although bearing in mind that only the unbound fraction of the total protein (or [Pub] = [Pt] − [Pb]) will participate in this equilibrium. For simplicity, we have used with this purpose the sequential monomer addition model with m = ∞ and assuming that the specific fluorescence of unbound oligomers (sFo) is independent of the oligomer size. Thus, the dependence of total fluorescence intensity (Fv) on the lipid vesicle concentration ([Vt]) will be described by

$$Fv = [Pb]sFb + [P]sFm + ([Pt] - [Pb] - [P])sFo \quad (16)$$

where the concentration of membrane-bound protein ([Pb]) is given by eq 15, while the concentration of free monomeric protein ([P]) is given by [P] = ([Pt] − [Pb])/(1 + K([Pt] − [Pb]).

If considering the fluorescence intensities in the presence of vesicles (Fv) relative to those in their absence (Fvo):

$$\frac{Fv}{Fvo} = \frac{[Pb]sFb + [P]sFm + ([Pt] - [Pb] - [P])sFo}{[Pvo]sFm + ([Pt] - [Pvo])sFo} \quad (17)$$

where the concentration of monomeric protein in the absence of vesicles is [Pvo] = [Pt]/(1 + K[Pt]).

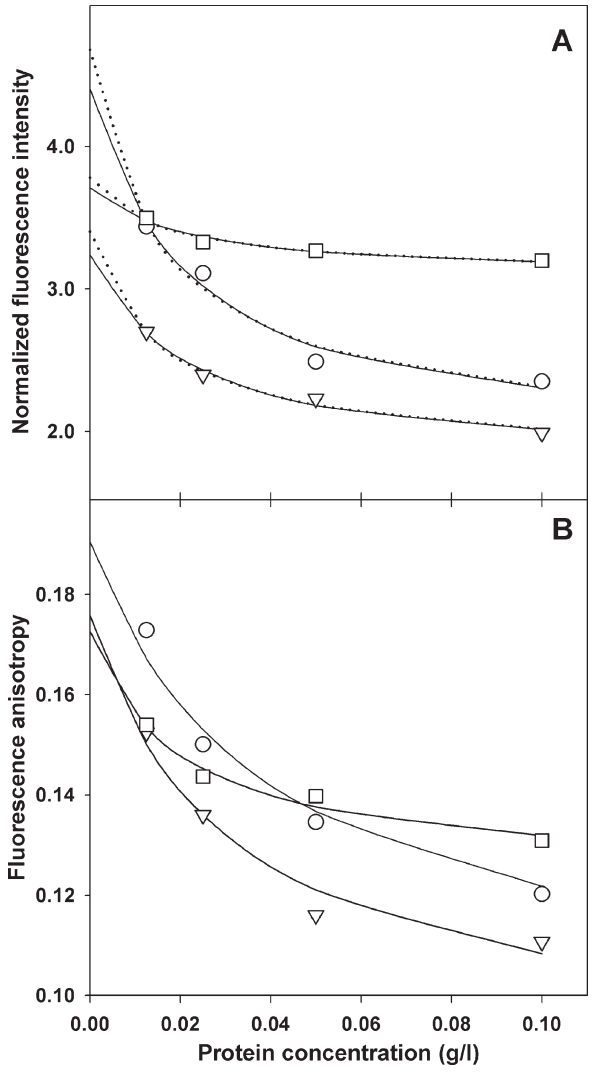

FIGURE 1: Effect of oligomerization on the tryptophan fluorescence intensity and anisotropy of apoAI single tryptophan mutants. The emission intensity normalized by the protein concentration (A) and fluorescence anisotropy (B) of W@93 (circles), W@104 (triangles), and W@108 (squares) were measured at different protein concentrations. Solid lines are best fits of the monomer−dimer−tetramer−octamer oligomerization model with the equilibrium constants reported by Vitello and Scanu (*19*) and supposing that homoquenching and homotransfer efficiency are independent of oligomer size for $n \geq 2$ (condition A2 with fixed Kn in Table 2). Dotted lines in (A) are best fits for the model of sequential monomer addition with $m = \infty$ (condition C2 with $m = \infty$ in Table 2).

Taking into account that $sFo = sFm/(1 + Khq)$, eq 17 can be rearranged as follows:

$$\frac{Fv}{Fvo} = \{([sFb/sFm][Pb](Khq+1)(K([Pb]-[Pt])-1)+([Pt]-[Pb])(K([Pb]-[Pt])-Khq-1))(K[Pt]+1)\}/\{[Pt](K[Pt]+Khq+1)(K[Pb]-[Pt])-1)\} \quad (18)$$

This function combined with eq 15 was fitted to the experimentally obtained data of fluorescence intensity as a function of lipid vesicle concentration in order to calculate the [sFb/sFm] ratios for each mutant and kind of quencher in the vesicles. For this fit, the parameters K and Khq were fixed to those obtained from the fit of combined eqs 5 and 9 to the variation of the fluorescence intensities of the mutants as a function of their concentration in solution. It was also assumed that vesicle binding is affected neither by mutations nor by the presence of spin-labeled lipids in the vesicles, and global fits were made to the data of the three mutants with all kinds of vesicles (containing or not spin-labeled lipids) in order to calculate single Kd and N values.

Application of the Parallax Method To Estimate the Membrane Insertion Depth of W Residues. According with Chattopadyay and London (*22*), the ratio of quenched (F) to unquenched (Fo) fluorescence intensity of a fluorophore buried in a membrane bilayer is related to the quencher and fluorophore localization by

$$F/F0 = e^{\pi C((Lc-Zc)^2-(Rc^2-X^2))} \text{ if } ((Lc-Zc)^2+X^2)^{1/2} \leq Rc \quad (19)$$

Here, Rc is the critical radius of a circle around the paramagnetic group within quenching is effective, X is the minimal lateral distance at which fluorophore and quencher can approximate, Lc and Zc are the distances from the bilayer center of quencher and fluorophore respectively, and C is the quencher concentration in molecules per area units. This relationship will be fulfilled if the average distance between fluorophore and quencher is shorter than the critical radius Rc; otherwise, F/Fo will be 1. If no restriction exists for the lateral approximation between fluorophore and quencher, as expected if the W residues are totally exposed to the bilayer lipids, X will be equal to zero.

Concerning proteins with reversible interaction with membranes as apoAI, the F/F0 ratio should be obtained at limiting conditions where 100% of the protein is membrane bound. In this case, F/F0 was obtained from

$$F/F0 = sFb/sFb0 = [sFb/sFm]/[sFb/sFm]0 \quad (20)$$

where [sFb/sFm] and [sFb/sFm]0 were obtained by fitting eq 10 to the fluorescence intensity data obtained with vesicles containing spin-labeled lipids or without quencher, respectively.

In order to calculate the distance from the bilayer center of the fluorophore (Lc) knowing the localization of the quencher and its quenching efficiency, it is also necessary to know the values of Rc (or Rc and X). For obtaining a solution independent of Rc and X, Chattopadyay and London (*22*) have used the ratio of the fluorescence intensities with two differently located quenchers. Another strategy is to fit by nonlinear regression directly eq 18 to the experimental data obtained by several quenchers. This approach is similar to that proposed by Ladokhin (*23*); it allows the direct estimation of the values for $Rc^2 - X^2$ (or for Rc if it is assumed that $X = 0$). Moreover, with this approach it is not necessary to know precisely the quencher concentration per area unit (C) since it is obtained in the fit. It is worth noting that C cannot be simply estimated in vesicles of phospholipid/cholesterol mixtures due to the uncertainness introduced by the cholesterol condensing effect.

RESULTS

Characterization of the Mutants. SDS−PAGE analysis indicated that purity of the final protein preparations was higher than 95% while MALDI-TOF analysis confirmed the identity of the mutants (see Supporting Information). The potential effect of mutations on the protein folding was checked by far-UV CD spectroscopy. The spectra of W@93, W@104, and W@108 were similar to those obtained for W@0 or wild-type apoAI (results not shown).

To check the functionality of these mutants, their ability to clear multilamellar vesicles of DMPC was compared with that of

Table 1: Tryptophan Fluorescence Emission of W@93, W@104, and W@108 in the Unfolded, Lipid-Free, and Membrane-Bound States

	unfolded state[a]		lipid-free folded state[b]			membrane-bound[c]	
mutant	λ max (nm)	intensity at 0.1 mg/mL[d]	λ max (nm)	intensity at 0.1 mg/mL[d,e]	intensity at 0.04 mg/mL	λ max (nm)	intensity at 0.04 mg/mL[d,f]
W@93	350	5.00	333	3.53 (0.71)	2.33	339	1.87 (0.80)
W@104	350	5.02	343	3.40 (0.68)	2.07	341	3.95 (1.91)
W@108	351	5.05	333	6.61 (1.31)	3.11	334	4.94 (1.59)

[a]For the unfolded state, spectra were acquired at a protein concentration of 0.1 mg/mL in 3.0 M guanidine hydrochloride and 25 mM sodium phosphate, pH 7.4. [b]For the lipid-free state, spectra were acquired at a protein concentration of 0.1 and 0.04 mg/mL in 25 mM sodium phosphate, pH 7.4. [c]For the membrane-bound state, spectra were acquired at a protein concentration of 0.04 mg/mL in the presence of POPC/cholesterol large unilamellar vesicles (final concentration: 2.5 mM POPC, 0.625 mM cholesterol) in 25 mM sodium phosphate, pH 7.4. [d]Given values are the relative fluorescence intensities at the corresponding λ max. Those for the membrane-bound state were corrected by inner filter effects. [e]Values within parentheses are those relative to the unfolded state. [f]Values within parentheses are those relative to the same protein concentration in the folded lipid-free state.

W@0 or the wild-type protein. All of the mutants, inclusive W@0, clear DMPC vesicles with similar rate among them but with lower rate than the wild-type protein (results not shown). It is to note that W@108 contains the wild-type sequence at the central apoAI repeats. Then, the decreased rate in clearing DMPC vesicles cannot be attributed to the mutations in the central region, and it should be due to one of the other substitutions present in these mutants (W8 → F, W50 → F, or W72 → F). In spite of a lower rate, the maximal clearing efficiency of all the mutants is not different from that observed for wild-type apoAI. Moreover, binding to POPC vesicles or self-association abilities are not affected by the mutations (see below). Together with the data of CD spectroscopy, these facts indicate that all of the mutants adopt a configuration similar to that of the wild-type protein both in the lipid-free and in the membrane-bound states.

Tryptophan Fluorescence of W@93, W@104, and W@108 in the Lipid-Free State. Evidence That the Central Y Helical Repeat Pair Participates in the Oligomerization of ApoAI in Aqueous Solution. The W emission spectra of W@93, W@104, and W@108 were acquired at a concentration of 0.1 mg/mL in their folded and unfolded states (i.e., in the absence or in the presence of 3 M guanidine hydrochloride), and spectral data are summarized in Table 1. The three mutants have very similar W fluorescence spectra and quantum yield in the unfolded state. In the folded state, the W of W@104 is in a more polar environment than W of W@93 and W@108, as is indicated by a longer wavelength of its emission maxima. As expected, unfolding with 3 M guanidine hydrochloride results in a red shift of W emission for the three mutants. For W@108, as generally observed for most proteins, the red shift of W fluorescence emission in unfolding is accompanied by a decrease in quantum yield. Just the opposite, denaturation of W@93 and W@104 by guanidine hydrochloride results in increased fluorescence intensity. This fact indicates that some process leading to a decreased emission of W@93 and W@104 in the folded state is released in the unfolded state.

It is well-known that apoAI self-associates in aqueous solution forming dimers and higher oligomers (*19*, *24*−*26*). If the intermolecular distance between homologous W residues in oligomers is short enough, fluorescence intensity could be decreased by W−W interaction leading to some homoquenching process as the formation of nonfluorescent dark complexes (*18*). The disruption of oligomers evoked by guanidine hydrochloride denaturation would result in an enhancement of fluorescence intensity by releasing intermolecular W−W interactions and homoquenching. Interactions at short distances between identical fluorophores like W can also result in resonance energy homotransfer. Pure resonance energy homotransfer, however, is not expected to affect the quantum yield, although it would decrease the fluorescence anisotropy (*18*). In order to assess if intermolecular W−W interaction occurs in the oligomeric state of these apoAI mutants, fluorescence intensity and anisotropy were measured at variable protein concentrations. Since an increase in protein concentration would shift the equilibrium toward a higher proportion of larger oligomers, this should result in a decreased quantum yield and/or anisotropy if some W−W interaction occurs in the oligomeric state. Figure 1 shows that for the three mutants, but in particular for W@93 and W@104, fluorescence anisotropy and normalized intensity decrease when protein concentration is increased. No appreciable change in the wavelength for the emission maxima of the three mutants was observed when changing the protein concentration (data not shown), indicating that the environment polarity of W residues is not affected by oligomerization. Thus, anisotropy and intensity changes should be attributed to W−W energy homotransfer and some homoquenching process as dark complex formation, respectively. For W−W homotransfer, R0 values range in the order of 4−15 Å depending on the environment (*20*). The estimated R0 values for these mutants are about 10 Å (see Experimental Procedures). Thus, this phenomenon should be undetectable at distances larger than 2.5 R0 (or 25 Å). Dark complex formation would require collision between W residues, and thus the average distance between W residues in oligomers should be even shorter than that required for evoking homotransfer. Thus, these qualitative results indicate that the central Y helix pairs of apoAI are close together in dimers or higher oligomers.

In order to obtain a quantitative estimation of these intermolecular distances, it is necessary to assume a model for the self-association equilibrium as well as for the homoquenching and homotransfer dependence on the oligomer size to fit the corresponding equations to the experimental data. The oligomerization equilibrium of apoAI in aqueous solution has been studied by sedimentation equilibrium ultracentrifugation by Vitello and Scanu (*19*). These data indicate that the degree of association should be of at least 6, and they are well described by a monomer−dimer−tetramer−octamer equilibrium. On the other hand, cross-linking experiments (*24*, *25*) suggest the presence of trimers (and possible pentamers), indicating that all discrete oligomers increasing their size in one step could be present in the equilibrium (sequential monomer addition model). Both possibilities have been here considered.

On the other hand, the homoquenching and homotransfer dependence on the oligomer size can be very complex in higher oligomers, where several intermolecular distances among

Table 2: Parameters Obtained by Fitting the Monomer−Dimer−Tetramer−Octamer Equilibrium Model to the Fluorescence Intensity and Anisotropy Dependence on the Protein Concentration

	mutant																	
	W@93					W@104					W@108							
parameter[a]	sF1	Khq	r1	Ra	Rb	sF1	Khq	r1	Ra	Rb	sF1	Khq	r1	Ra	Rb	K (L/g)	$\sum\delta FN \times 10^2$	$\sum\delta r \times 10^4$
(A) Equidistant Separation of W Residues in Oligomers[b]																		
fixed Kn[c]	3.67	0.18	0.181	12.6	11.6	2.79	0.10	0.159	13.1	11.9	3.50	0.022	0.156	18.3	16.4		4.15	1.63
$Kn = K^{n-1}$	4.26	0.21	0.201	12.7	11.9	3.10	0.12	0.177	13.0	11.9	3.62	0.028	0.164	17.7	16.0	166	3.07	0.63
$Kn = nK^{n-1}$	4.75	0.26	0.219	12.1	11.5	3.33	0.15	0.192	12.4	11.6	3.69	0.032	0.170	17.2	15.6	203	3.18	0.58
(B) Homoquenching and Homotransfer Efficiency Independent of Oligomer Size[d]																		
fixed Kn	4.40	1.30	0.189	≤4[e]	≤4	3.24	0.81	0.172	≤4	≤4	3.71	0.20	0.168	12.2	11.2		2.74	0.86
$Kn = K^{n-1}$	4.65	1.45	0.193	≤4	≤4	3.38	0.91	0.175	≤4	≤4	3.77	0.22	0.171	12.1	11.2	78.2	2.94	0.81
$Kn = nK^{n-1}$	5.11	1.72	0.198	≤4	≤4	3.65	1.07	0.181	≤4	≤4	3.89	0.26	0.176	12.0	11.1	62.9	3.10	0.82

[a]Calculated parameters were as follows: the specific fluorescence intensity of monomers (sF1), the homoquenching constant (Khq), the fluorescence anisotropy of monomers, and the estimated distance (in Å) separating intermolecular W residues considering no contribution of depolarizing rotation (Ra) or considering such contribution (Rb). When not fixed, the equilibrium constant (K) was also obtained and given in units of g^{-1} L. The summations of the squares of the residuals are given for the normalized fluorescence ($\sum\delta FN$) or the anisotropy ($\sum\delta r$) data. Equations used were (1) $[Pt] = [P] + K2[P]^2 + K4[P]^4 + K8[P]^8$, (2) $FN = ([P]sF1 + K2[P]^2sF2 + K4[P]^4sF4 + K8[P]^8sF8)/[Pt]$, and (3) $r = ([P]sF1r1 + K2[P]^2sF2r2 + K4[P]^4sF4r4 + K8[P]^8sF8r8)/[Pt]$. [b]For this situation, $sFn = sF1/(1 + (n - 1)Khq)$ and $rn = r1(Ra^6 + R0^6)/(Ra^6 + nR0^6)$ without considering the contribution of rotational depolarization, or $rn = r0r1(Rb^6 + R0^6)^2/(r0Rb^{12} + Rb^6R0^6(r1(n - 1) + 2r0) + nr0R0^{12})$ if considering such contribution. In the last case, a value of 0.315 was used for the fundamental anisotropy (r0). Foster's distances (R0) were 10.41, 10.18, and 11.05 Å for W@93, W@104 and W@108, respectively. [c]In this case, the equilibrium constants K2, K4, and K8 were fixed to the values reported by Vitello and Scanu (*19*). [d]For this situation, $sFn = sF1$ and $rn = r1$ for monomers, and $sFn = sFo = sF1/(1 + Khq)$ and $rn = ro = r1(Ra^6 + R0^6)/(Ra^6 + 2R0^6)$ (without depolarizing rotation) or $ro = r0r1(Rb^6 + R0^6)^2/(r0Rb^{12} + Rb^6R0^6(r1 + 2r0) + nr0R0^{12})$ (with depolarizing rotation) for oligomers of size $n \geq 2$. [e]Since energy transfer efficiency is relatively insensitive to R when $R \leq 0.4$ R0, distances below 4 Å are not significantly different from zero.

W residues should be considered. However, this can be simplified by assuming these two extreme situations: (a) all of the W residues in the oligomer are equidistant and interact equally with each other or (b) homoquenching and/or homotransfer in oligomers is due only to the interaction between pairs of W residues which are far enough from other W residues (or W pairs). It is to note that even if both assumptions are not totally true, the first one will overestimate while the second will underestimate the closest approximation between the W residues of these mutants in the oligomers. Thus, they will give respectively the highest and lowest limits for the estimation of the intermolecular distances of the reported positions in the self-associated apoAI.

Equations corresponding to these extreme situations (given in Experimental Procedures) combined with those corresponding to different oligomerization equilibrium models were fitted to data in Figure 1. The monomer−dimer−tetramer−octamer equilibrium was first considered. Results of the fittings for this model are shown in Table 2 where the calculated parameters and the sum of the squares of residuals are listed. When fixing the equilibrium constants to the values reported by Vitello and Scanu (*19*), a relatively poor fit is obtained when assuming that all of the W residues in oligomers are equidistant and interacting equally, but a good fit to both data (intensity and anisotropy) is obtained by assuming that homoquenching and homotransfer efficiency do not depend on the oligomer size. This fact indicates that dimerization of apoAI results in homoquenching and homotransfer, but no further decrease in fluorescence intensity and anisotropy is produced when dimers arrange in tetramers or octamers. If assuming this model, the intermolecular distances between W residues in dimers are ≤4 Å for W@93 and W@104 and about 11 Å for W@108.

If the equilibrium constants are not fixed and allowed to be calculated by the wizard, relatively good fits are obtained for the monomer−dimer−tetramer−octamer equilibrium in both situations (equidistant W separation or homoquenching/homotransfer efficiency independence of oligomer size) even if the equilibrium constants for each oligomerization step are supposed interrrelated by $Kn = K^{n-1}$ or by $Kn = n K^{n-1}$. These fits, however, result in very similar calculated intermolecular W−W distances to those obtained by fixing the values for the equilibrium constants: about 12 Å for W@93 and W@104 and 16 Å for W@108, if assuming equidistant W separation, or ≤4 Å for W@93 and W@104 and 11 Å for W@108 when assuming homoquenching/homotransfer independence of the oligomer size.

Other oligomerization equilibrium models fit well to the experimental data, as sequential monomer or dimer addition (see Table in Supporting Information). While the maximal oligomer size m is maintained in 8, these fits result in similar intermolecular W−W distances to those arising from the monomer−dimer−tetramer−octamer equilibrium. For the assumption of equidistant W separation, the estimated distances are around 50% larger when m is increased until 64, but they are independent of m if assuming homoquenching/homotransfer independence of the oligomer size. The convergent series arising from supposing $m = \infty$ fit also very well to the data, in particular to the fluorescence intensity ones.

Tryptophan Fluorescence of W@93, W@104, and W@108 in the Membrane-Bound State. In order to obtain information about the conformation of the central 3−4 helix pair in the membrane-bound state, W fluorescence spectra of W@93, W@104, and W@108 were measured in the presence of lipid vesicles. Since apoAI membrane binding is facilitated by cholesterol (*8*), unilamellar vesicles of POPC/cholesterol (4/1 molar ratio) were used with this aim. According with previously published constants for apoAI binding to egg PC/cholesterol vesicles (*8*), more than 90% of the proteins should be bound to the vesicles in the used apoAI and vesicle concentrations (0.04 mg/mL and 2.5 mM, respectively). The wavelength for the emission maxima and the intensities relative to those of the same protein concentration in the lipid-free state are given in Table 1. No appreciable shift is observed for the emission of W@104 and W@108, indicating that the membrane binding process does not

change the environment polarity for these residues. The residue at position 104 senses a more polar environment than residue 108 in both lipid-free and membrane-bound states. On the other hand, lipid vesicle addition results unexpectedly in a red shift for the emission of W@93, indicating a relatively more polar environment in the membrane-bound compared with the lipid-free state.

It is also shown in Table 1 that while the emission intensity for W@104 and W@108 is increased (about 1.6 and 1.9 times, respectively) in the membrane-bound state, it is decreased by about 20% in W@93. As previously shown, apoAI binding to lipid vesicles is accompanied by a shift in the oligomerization equilibrium (*12*). Dimers and tetramers are the predominant membrane-bound species while membrane-bound monomers are undetectable. This fact, together with the increased quantum yield observed here for W@104 and W@108, indicates that the homoquenching process detected in lipid-free oligomers for these mutants is absent in membrane-bound oligomers. In the case of W@93, the absence of homoquenching in membrane-bound oligomers cannot be totally discarded. However, the small decrease in emission intensity can be easily attributed to the increase in environment polarity reported by its red-shifted emission. Moreover, a higher decrease in quantum yield should be expected for membrane-bound oligomers if the homoquenching efficiency found in lipid-free oligomers is maintained. Thus, even for W@93 the homoquenching efficiency should be decreased in membrane-bound dimers or tetramers as compared with lipid-free oligomers. Unfortunately, anisotropy measurements in the presence of high amounts of lipid vesicles are very imprecise due to the high level of scattered light, and the approach used for estimating the homotransfer efficiency in lipid-free oligomers is inapplicable to estimate intermolecular distances in the membrane-bound state. However, the decrease in homoquenching efficiency suggests that intermolecular distances between homologous residues 93−93, 104−104, and 108−108 are larger in membrane-bound dimers or tetramers as compared with oligomers in aqueous solution.

Quenching of W@93, W@104, and W@108 Tryptophan Fluorescence by Lipid Vesicles Containing Spin-Labeled Lipids. With the aim of obtaining information on the membrane insertion topology of the central 3−4 α-helical repeat, the tryptophan fluorescence quenching efficiency by spin-labeled phospholipid analogues with the paramagnetic group located at different positions was measured for W@93, W@104, and W@108. Tryptophan emission spectra of each mutant were measured in the presence of increasing concentrations of POPC/cholesterol (4/1 in moles) unilamellar vesicles containing or not 20% in moles of different spin-labeled phosphatidylcholines (tempo-PC and 5-, 10-, or 14-doxyl-PC) or a spin-labeled cholesterol analogue (doxylcholestane). After background subtraction and correction by inner filter, fluorescence intensity was obtained by spectral integration.

Figure 2 shows the variation of the emission intensity (relative to that obtained for the lipid-free state) as a function of vesicle concentration. The addition of vesicles containing no quencher decreases the fluorescence intensity of W@93 but increases that of W@104 and W@108 in agreement with data shown in Table 1. The presence of tempo-PC and 5-, 10-, or 14-doxyl PC affects in a differential way the fluorescence intensity of each mutant. For W@93, quenching efficiency follows the order 5-doxyl-PC > tempo-PC ≈ 10-doxyl-PC > 14-doxyl-PC. For W@104 the order is 5-doxyl-PC ≈ 10 doxyl-PC > 14-doxyl-PC > tempo-PC while for W@108 is tempo-PC > 5-doxyl PC > 10-doxyl-PC > 12-doxyl-PC. Inspection of these data indicates that the W

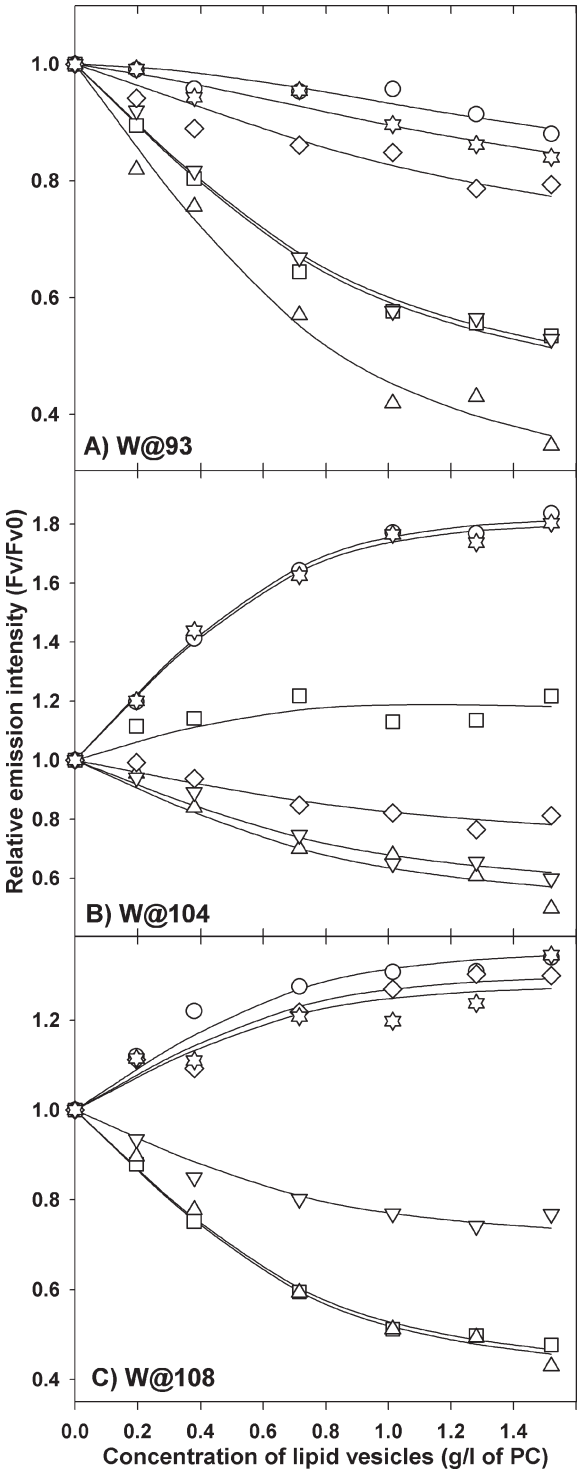

FIGURE 2: Influence of binding to lipid vesicles containing spin-labeled lipids on the tryptophan emission intensity of W@93 (A), W@104 (B), and W@108 (C). The emission intensity of the mutants at a concentration of 0.1 g/L in the presence of variable amounts of lipid vesicles is given relative to that obtained in the absence of vesicles. Used vesicles were as follows: (a) containing no quencher, POPC/cholesterol 4/1 in molar ratio (circles); (b) containing spin-labeled phosphatidylcholines, POPC/spin-labeled PC/cholesterol 3/1/1 in molar ratio, where spin-labeled PC is tempo-PC (squares), 5-doxyl-PC (triangles up), 10-doxyl-PC (triangles down), and 14-doxyl-PC (diamonds); (c) containing spin-labeled cholesterol, POPC/doxylcholestane 4/1 in molar ratio (stars). Lines are best fits of combined eqs 15 and 18 to data.

residue of W@93 locates at the lipid bilayer at a depth similar to that of the paramagnetic group of 5-doxyl-PC, while the W of W@104 locates deeper (approximately between 5- and

10-doxyl-PC) and W@108 more superficially (approximately between tempo-PC and 5-doxyl-PC). On the other hand, the presence of doxylcholestane in the vesicles does not quench significantly the W emission of the mutants, indicating that this cholesterol analogue would be excluded from the environment of the central helical domain of apoAI.

The location of a W residue of a protein or peptide can be estimated by means of the parallax method described by Chattopadhyay and London (*22*) and further adapted by Ladokhin (*23*). In order to apply this method to the present situation of a protein interacting reversibly with the membrane, it is necessary to estimate the ratio of fluorescence intensities in the presence and absence of quenchers (F/F0) in the limiting situation when 100% of the protein is membrane bound. Thus, F/F0 ratios were obtained by fitting eqs 14 and 17 (see Experimental Procedures) to data in Figure 2. A global fit to the data of the three mutants and all kinds of quenchers in the vesicles were used in order to calculate single values for the binding parameters Kd and N (assuming that they are affected neither by the presence of spin-labeled lipids in the vesicles nor by the mutations in apoAI) and the specific fluorescence intensities of the bound proteins relative to their fluorescence intensity in the free monomeric state (sFb/sFm ratios). The obtained parameters are listed in Table 3. Calculated Kd and N values are in the same order as those obtained by Yokoyama et al. (*8*) for the binding of apoAI to vesicles of egg PC/cholesterol (4/1 molar ratio).

The sFb/sFm values obtained with vesicles containing quencher were then normalized by the values obtained in the absence of quencher to obtain the ratio of quenched to unquenched emission (F/F0) of the membrane-bound proteins. These data are also listed in Table 3, and they were used to estimate the depth of the mutant W residues in the membrane lipid bilayer through a modification of the parallax method described by Chattopadyay and London (*22*). In Figure 3, the F/Fo ratios are plotted as a function of the quencher distance from the bilayer center. The lines represent the best fit of eq 18, and the parameters obtained are listed in Table 4. The quencher concentration per area unit (C) obtained from the fit is in agreement with that which can be estimated considering the used quencher molar ratio and a molecular area for PC somewhat condensed by the presence of cholesterol. The values of $Rc^2 - X^2$ are also in the expected range according to those previously reported (*22*, *27*, *28*). It is to note, however, that the value obtained for W@93 is lower than those for the other mutants. As there is no apparent reason for a change in Rc with the same fluorophore−quencher pair, it is reasonable to attribute this change to a different lateral accessibility of the quencher to the W residue in this mutant. An estimation for X in each mutant is given in Table 4, by assuming a value of 12 Å for Rc as previously reported for this kind of quencher (*22*, *27*, *28*). Since Rc and X cannot be measured independently, these estimations for X are approximate, but they suggest that quencher accessibility to the tryptophan residue is lower in W@93 than in W@104 or W@108. This fact is in agreement with the observation that tryptophan emission in W@93 is red shifted and less intense than that of the other mutants. Both data suggest that W of W@93 is less accessible to the lipid environment than W of W@104 and W@108.

Independently of the lateral accessibility to quenchers from the lipid phase, data in Table 4 discard that helices 3 and 4 are embedded into the membrane with their long axis parallel to the lipid bilayer surface. The obtained distances from the bilayer center for the W residue of these mutants (13.4, 10.5, and 15.7 Å for W@93, W@104, and W@108, respectively) indicate a rather superficial location for residue 108, while residue 104 locates about

Table 3: Parameters Resulting from Fitting a Simple Binding Model to the Fluorescence Intensity Dependence on the Concentration of Vesicles Containing Spin-Labeled Lipids

mutant	quencher in vesicles	sFb/sFm ± standard error[a]	sFb/sFb0 or F/F0[b]
W@93	none	0.414 ± 0.010	1
	tempo-PC	0.194 ± 0.015	0.468
	5-doxyl-PC	0.105 ± 0.018	0.254
	10-doxyl-PC	0.199 ± 0.015	0.481
	14-doxyl-PC	0.346 ± 0.011	0.836
	doxylcholestane	0.390 ± 0.010	0.942
W@104	none	1.142 ± 0.020	1
	tempo-PC	0.707 ± 0.010	0.618
	5-doxyl-PC	0.283 ± 0.016	0.248
	10-doxyl-PC	0.317 ± 0.015	0.277
	14-doxyl-PC	0.429 ± 0.012	0.375
	doxylcholestane	1.129 ± 0.019	0.988
W@108	none	1.171 ± 0.017	1
	tempo-PC	0.323 ± 0.023	0.276
	5-doxyl-PC	0.313 ± 0.023	0.267
	10-doxyl-PC	0.585 ± 0.017	0.499
	14-doxyl-PC	1.122 ± 0.016	0.958
	doxylcholestane	1.100 ± 0.016	0.939
binding parameters[a]			
Kd (g/L)		0.0188 ± 0.006	
N (g of protein/g of PC)		0.134 ± 0.008	

[a]Combined eqs 12 and 16 were globally fitted to the data in Figure 3, with the following fixed parameters: [Pt] = 0.1 g/L, K = 62.7 L/g, and Khq = 1.42, 0.90, or 0.22 for W@93, W@104, or W@108, respectively. In this way, single values for the binding parameters (Kd and N) as well as the ratios sFb/sFm for each mutant and kind of quencher were calculated. [b]The ratios sFb/sFm for each kind of quencher were normalized by the ratio obtained with vesicles containing no paramagnetic quencher.

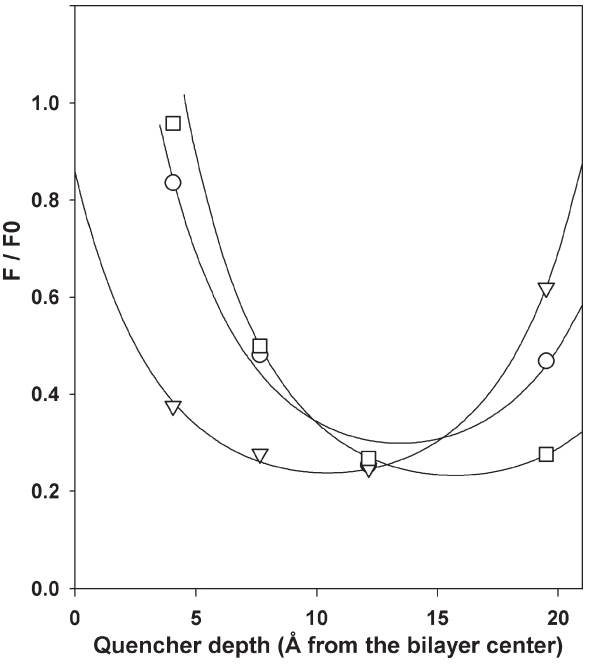

FIGURE 3: Influence of spin-group depth at the lipid bilayer on the fluorescence quenching of single tryptophan mutants. The F/F0 ratios, obtained from limiting conditions where the totality of the protein is membrane-bound, are plotted as a function of the quencher distance from the bilayer center for W@93 (circles), W@104 (triangles), or W@108 (squares). Lines represent best fits of eq 19 to data.

Table 4: Calculation of Membrane Insertion Depth for W Residues of ApoAI Mutants

Fixed Parameters: Distance from Bilayer Center (Lc, in Å) for the Paramagnetic Group of Spin-Labeled Phospholipids[a]			
tempo-PC	5-doxyl-PC	10-doxyl-PC	14-doxyl-PC
19.5	12.15	7.65	4.05

Parameters Estimated by Nonlinear Regression					
mutant	C (molecules/Å^2)	Zc (Å)	(Rc^2 − X^2)[b](Å^2)	Rc[c](Å)	X[d](Å)
W@93	0.0037 ± 0.0004	13.45 ± 0.31	102.9 ± 7.3	10.1	6.4
W@104		10.46 ± 0.33	122.4 ± 9.1	11.1	4.6
W@108		15.71 ± 0.58	124.3 ± 12.8	11.1	4.4

[a]The values of Lc for 5- and 10-doxyl-PC were taken from ref *22*. The value corresponding to tempo-PC was from ref *28*. The value for 14-doxyl-PC was estimated considering that the distance from the bilayer center decreases by 0.9 Å for each C atom in the phospholipid fatty acyl chain as reported by the same authors (*22*). [b]Calculated directly from the regression. [c]These values of Rc were obtained assuming X = 0, meaning no restriction for the lateral accessibility of quenchers to the W residues. [d]The given values for X were obtained assuming for Rc a value of 12 Å as reported for these quenchers (*22*).

5.2 Å more deeply. The difference in depth between residues 104 and 108 is not very different from that expected for the advance of an α-helix through four residues (6 Å), indicating that helix 4 locates with its long axis almost perpendicularly to the membrane surface. On the other hand, residue 93 of helix 3 locates at an intermediate depth between residues 104 and 108 of helix 4. This fact indicates the existence of a turn separating both helices (very probably around proline 99) and that helix 3 is antiparallel to helix 4 and also nearly perpendicular to the membrane surface.

DISCUSSION

The main goal of this study was obtaining information about the membrane insertion topology of the central apoAI class Y helical repeat pair 3−4, as well as inferring the nature of the conformational change in this region between the lipid-free and membrane-bound states. The insertion depths of W residues for three single W apoAI mutants were estimated by using a modification of the parallax method, which is based on the accessibility to paramagnetic quenchers of known location in the bilayer. The results show a superficial location for the W residue of W@108 (15.7 Å from the center of the lipid bilayer) and a deeper location for W residues in W@93 and W@104 (13.4 and 10.5 Å from the bilayer center, respectively). The difference in depth of 5.2 nm observed for the reporter W residue at positions 104 and 108 indicates that the helical repeat 4 would be located with its long axis roughly perpendicular to the membrane surface. The intermediate depth estimated for W in W@93 indicates the presence of a turn (probably around proline 99) and that repeat 3 would be located antiparallel to repeat 4.

Considering that polar faces of repeats 3 and 4 are much wider than their nonpolar faces, the insertion of an isolated 3−4 antiparallel repeat pair with the helix axis perpendicular to the membrane surface is very unlikely since it would result in the exposure of polar residues to the hydrophobic environment. Such insertion mode, however, can be possible if more helices interact together to form a membrane-inserting bundle. The participation of other apoAI repeats in such membrane-inserting bundle is discarded by the fact that only the 3−4 repeat pair (residues 87−112) was labeled by the photoactivable ^{125}I-TID/PC reagent incorporated into the membrane (*11*). However, it was shown that apoAI forms dimers or tetramers in the membrane-bound state while membrane-bound monomers are undetected (*12*). Thus, it is likely that two pairs of 3−4 repeats would interact together to form an intermolecular bundle as shown in the hypothetical model in Figure 4. Both repeats are shown totally in an α-helical structure as they are found in the crystal of Δ1−43 apoAI (*4*). Figure 4 remarks the distribution of charged residues, indicating that salt bridges could help to stabilize the membrane-inserted helix bundle with the total neutralization of free charges. Each repeat contains two positively charged (K94 and K96 in repeat 3 and K106 and K107 in repeat 4) and two negatively charged (E91 and E92 in repeat 3 and D102 and D103 in repeat 4) residues. In an α-helical configuration, the spatial charge distribution allows the formation of eight salt bridges, with each one of the helical repeats 3 bound through two saline bridges with each one of the repeats 4 (E91−K106 and K94−D102 bridges with one partner and E92−K107 and K96−D103 with the another). In this way, the total neutralization of charges would be possible.

Since this putative bundle is too short to span the lipid bilayer, a second question concerning the turn in the membrane interior should be considered. In such hydrophobic environment, all of the polar groups in the turn should be paired by hydrogen bonds in order to avoid an increase in the free energy. It is very likely that proline 99 plays a key role in the turn since it has no free NH group to form the conventional intrahelical NH·O=C hydrogen bond. It is well-known that proline residues induce kinks in membrane α-helices, and it was proposed that nonconventional C−H·O bonds would satisfy the hydrogen bond forming potential of carbonyl groups (*29*), which would otherwise be unfavorably exposed to hydrophobic surroundings. At both sides of Pro99 there are two residues with hydrogen bond forming groups in the lateral chain (Q98 and Y100). The hydrogen bond forming potential of these groups should also be satisfied in the hydrophobic environment, and they could play an important role in forming this turn in the membrane interior.

The present results also give strong evidence that the central class Y helical repeat pair 3−4 participates in the oligomerization of apoAI in aqueous solution. Intermolecular distances between homologous residues are short enough in the lipid-free oligomers to result in tryptophan fluorescence homoquenching and homotransfer, in particular for W@93 and W@104. From the homotransfer efficiency, these intermolecular distances were estimated to be shorter than 5 Å for residues 93 and 104 and about 12 Å for residues 108. It is to note that, in the monomeric apoAI, the hydrophobic helix faces where these residues are located would point toward the interior of the protein as suggested by the fluorescence properties of these single tryptophan mutants (in particular for W@93 and W@108). The short intermolecular distances observed in dimers would need some rearrangement or reorientation of these α-helices in the protein/protein contact region.

These intermolecular distances could not be estimated in the membrane-bound state. However, it can be concluded that W−W interactions leading to homoquenching are absent in membrane-bound oligomers of W@104 and W@108, and they occur with very low efficiency, if any, in the case of W@93. These facts indicate a considerable rearrangement of the 3−4 repeat pair between oligomers in aqueous solution compared with the membrane-bound ones. A possibility is that in lipid-free oligomers the Y helical 3−4 repeat pairs would interact with each other through the hydrophobic helix faces as outlined in Figure 5.

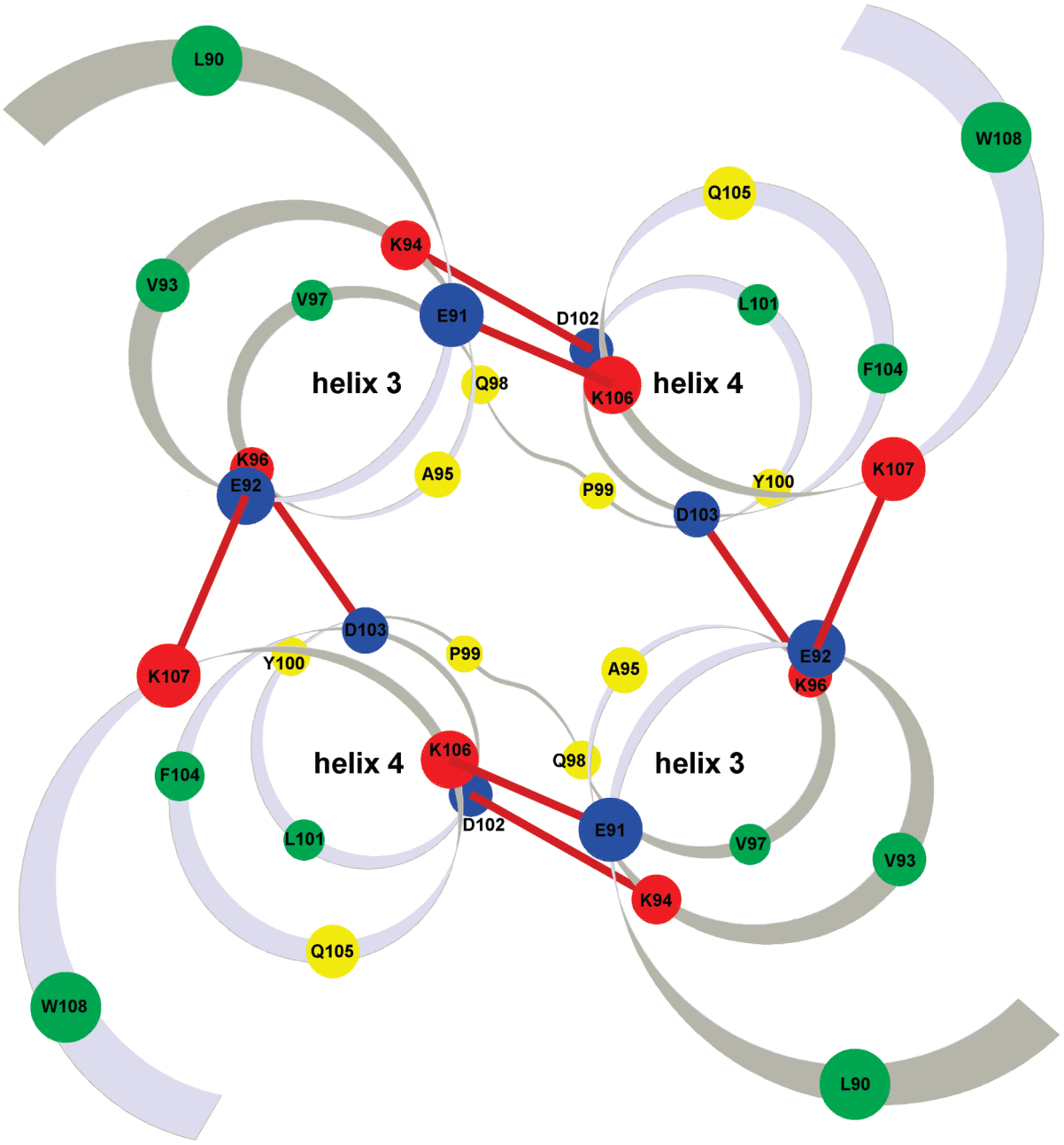

FIGURE 4: Hypothetical model for the membrane insertion of the central 3−4 repeat pair. Diagram illustrating an intermolecular four-helix bundle formed by two 3−4 repeat pairs inserted into the membrane with the long helix axes perpendicular to the membrane surface. The position of α-carbon atoms is shown by colored balls: green for hydrophobic, red for positively charged, blue for negatively charged, and yellow for neutral aminoacyl residues. Putative saline bridges are indicated by brown bars.

This would result in a very short distance between homologous residues belonging to the nonpolar helix face, making possible W−W collisions leading to homoquenching. In the inserted helix bundle, on the other hand, helix−helix interactions would occur through the polar helix faces laying the nonpolar faces out toward the lipid environment (Figure 4), precluding W−W collisions or interactions that lead to homoquenching.

Another observation arising from this work is the red-shifted emission of W@93 in the membrane-bound state compared with the lipid-free state, indicating that residue 93 is in a more polar environment in the membrane-bound state. Thus, the intermolecular helix−helix interaction through the nonpolar faces effectively shields this residue from exposure to water. In the membrane-inserted state, however, this residue located near the interface between the polar and nonpolar helix faces would be more exposed to water or near other polar residues of the helix bundle. This vision agrees with the additional observation that this residue seems to be less accessible to the spin-labeled lipids.

As previously reported (*11*, *12*), some programs (*30*) predict a structural analogy of the central apoAI repeats with ectatomin. Ectatomin is a dimer of two similar subunits forming a four-helix bundle. It is very soluble in aqueous solutions, though it inserts into lipid membranes forming an ion pore after considerable rearrangement of their amphipathic helices (*31*, *32*). A synthetic peptide with the sequence of the central apoAI region (AI 77−120) has been shown to have some structural and functional independence (*12*). It has a considerable helical content in aqueous solution that does not change when it binds to membranes where it is labeled by the photoactivable ^{125}I-TID/PC reagent with similar extension to that of apoAI. Similarly to

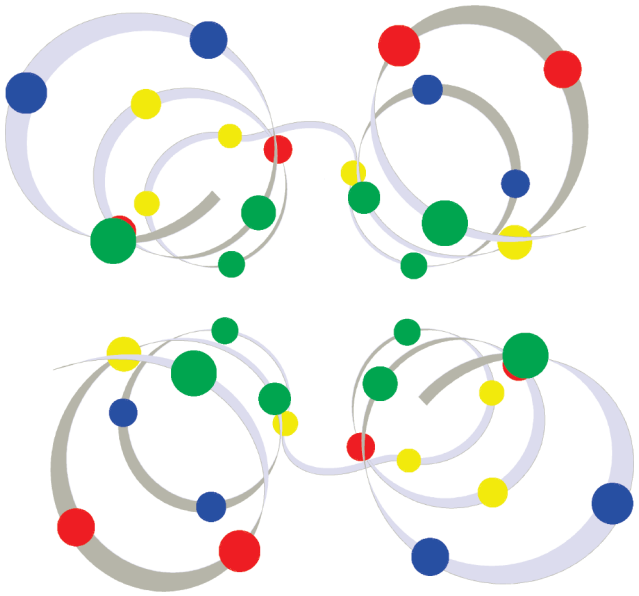

FIGURE 5: Diagram illustrating the possible arrangement of the intermolecular central Y-helix bundle in a dimer of apoAI in the lipid-free state. Color codes are as those given in Figure 4.

apoAI, this peptide promotes cholesterol efflux from cells and its desorption from artificial membranes (*12*). As observed here, the spin-labeled cholesterol analogue doxylcholestane was unable to evoke quenching of the W emission of W@93, W@104, and W@108. This fact indicates that this analogue would be excluded from the lipid environment of the central apoAI domain, and thus, it is possibly related with the ability of this domain to facilitate membrane cholesterol desorption.

The best known lipid-bound state of apoAI is when it forms discoidal HDL complexes (dHDL) containing two apoAI molecules. According to the currently accepted model of dHDL (*33*), two helical ring-shaped apoAI molecules wrap around a leaflet of a disk-like patch of lipid bilayer in an antiparallel orientation and rotationally aligned by interhelical salt bridges at helix 5 as in the crystal structure of Δ1−43 apoAI (*4*). This arrangement, known as LL5/5 extended double belt configuration, has been supported by several experimental (*15*, *34*−*38*) and computational (*39*−*41*) studies, although several deviations from the basic arrangement were detected by distance constraint determinations using FRET measurements or lysine chemical cross-link and mass spectroscopy. Such deviations were attributed to the presence of (a) more than one coexisting rotational registry (*37*, *42*, *43*) or (b) some helical regions folding back to form hairpin structures (*44*−*46*) and/or looping out from the dHDL surface (*47*−*49*). With minor variations, the general structural organization of apoAI was detected to be similar in discoidal or spherical HDL irrespective of the size and number of apoAI in the complex (*42*−*45*, *50*). Thus, it is to be expected that the general characteristics of the belt model should also apply to the present case of apoAI bound to lipid vesicles, in spite of a higher curvature radius of the vesicle surface in comparison with HDL.

The proposed intermolecular bundle of the central 3−4 helix pair will require a close intermolecular approximation of these helices, which is not possible in the LL5/5 extended conformation. Thus, some variation of this configuration should be present in the vesicle-bound state. The intermolecular approximation of helices 3−4 was detected here in lipid-free oligomers, and it was also revealed in discoidal and spherical HDL by the detection of several intermolecular lysine−lysine cross-links that do not fit the LL5/5 conformation (*35*, *37*, *43*−*45*). Then, the configuration of apoAI in the vesicle-bound state could be similar to one of those proposed in HDL to explain these cross-links, as the alternative LL5/2 registry (*37*, *43*) or the folding back of some helical regions to form a hairpin (*44*−*46*).

In spite of the expected conformational similarities, a striking difference between vesicle- and dHDL-bound apoAI is the different interaction with the lipid phase displayed by the central region where the 3−4 helix pair is present. As detected by hydrophobic photoactivable reagents, this is the unique apoAI region that deeply inserts into the lipid bilayer when the protein is bound to phospholipid vesicles, but it seems loosely bound to the lipids in dHDL complexes (*11*). Then, it is possible that in dHDL the intermolecular 3−4 helix pair bundle would acquire a conformation similar to that shown in Figure 5 with the helices interacting through their hydrophobic faces and thus avoiding its interaction with the HDL lipids.

It is worth noting that discoidal HDL can also bind to phospholipid membranes with variable affinity depending on their size and composition (*9*). Also in this case, the photoactivable ^{125}I-TID/PC reagent incorporated into the membrane reacts exclusively with the region corresponding to the 3−4 Y helical repeat pair (*11*). Thus, this region could act as a membrane-anchoring domain facilitating lipid exchange between membranes and dHDLs (*11*, *51*). Since the size and cholesterol content of dHDL affect the conformation and exposure degree of the central apoAI domain (*52*), these factors could modulate the formation of the putative membrane-inserting helix bundle and thus control its membrane affinity and lipid exchange ability.

In summary, we have shown in this work that the central Y helical apoAI repeats insert into the membrane with the long helix axis almost perpendicular to the membrane surface, thus explaining why this region is exclusively labeled by photoactivable reagents deeply located in the membrane lipid bilayer (*11*).

ACKNOWLEDGMENT

We thank Mrs. Laura Hernández for expert technical assistance and Mrs. Norma Tedesco for English revision and editing.

SUPPORTING INFORMATION AVAILABLE

Purity and quality controls of the apoAI mutant preparations by SDS−polyacrylamide gel electrophoresis and MALDI-TOF analysis, as well as complementary data to Table 2 where additional oligomerization equilibrium models were used in fittings. This material is available free of charge via the Internet at http://pubs.acs.org.

REFERENCES

1. Tang, C., and Oram, J. F. (2009) The cell cholesterol exporter ABCA1 as a protector from cardiovascular disease and diabetes. *Biochim. Biophys. Acta 1791*, 563–572.
2. Marcel, Y. L., and Kiss, R. S. (2003) Structure-function relationships of apolipoprotein A-I: a flexible protein with dynamic lipid associations. *Curr. Opin. Lipidol. 14*, 151–157.
3. Segrest, J. P., Jones, M. K., De Loof, H., Brouillette, C. G., Venkatachalapathi, Y. V., and Anantharamaiah, G. M. (1992) The amphipathic helix in the exchangeable apolipoproteins: a review of secondary structure and function. *J. Lipid Res. 33*, 141–166.
4. Borhani, D. W., Rogers, D. P., Engler, J. A., and Brouillette, C. G. (1997) Crystal structure of truncated human apolipoprotein A-I suggests a lipid-bound conformation. *Proc. Natl. Acad. Sci. U.S.A. 94*, 12291–12296.
5. Silva, R. A., Hilliard, G. M., Fang, J., Macha, S., and Davidson, W. S. (2005) A three-dimensional molecular model of lipid free apolipoprotein

A-I determined by cross-linking/mass spectrometry and sequence threading. *Biochemistry 44*, 2759–2769.
6. Thomas, M. J., Bhat, S., and Sorci-Thomas, M. G. (2008) Three-dimensional models of HDL apoA-I: implications for its assembly and function. *J. Lipid Res. 49*, 1875–1883.
7. Massey, J. B., and Pownall, H. J. (2008) Cholesterol is a determinant of the structures of discoidal high density lipoproteins formed by the solubilization of phospholipid membranes by apolipoprotein A-I. *Biochim. Biophys. Acta 1781*, 245–253.
8. Yokoyama, S., Fukushima, D., Kupferberg, J. P., Kézdy, F. J., and Kaiser, E. T. (1980) The mechanism of activation of lecithin:cholesterol acyltransferase by apolipoprotein A-I and an amphiphilic peptide. *J. Biol. Chem. 255*, 7333–7339.
9. Tricerri, M. A., Sanchez, S. A., Arnulphi, C., Durbin, D. M., Gratton, E., and Jonas, A. (2002) Interaction of apolipoprotein A-I in three different conformations with palmitoyl oleoyl phosphatidylcholine vesicles. *J. Lipid Res. 43*, 187–197.
10. Mishra, V. K., Palgunachari, M. N., Segrest, J. P., and Anantharamaiah, G. M. (1994) Interactions of synthetic peptide analogs of the class A amphipathic helix with lipids. Evidence for the snorkel hypothesis. *J. Biol. Chem. 269*, 7185–7191.
11. Córsico, B., Toledo, J. D., and Garda, H. A. (2001) Evidence for a central apolipoprotein A-I domain loosely bound to lipids in discoidal lipoproteins that is capable of penetrating the bilayer of phospholipid vesicles. *J. Biol. Chem. 276*, 16978–16985.
12. Toledo, J. D., Prieto, E. D., Gonzalez, M. C., Soulages, J. L., and Garda, H. A. (2004) Functional independence of a peptide with the sequence of human apolipoprotein A-I central region. *Arch. Biochem. Biophys. 428*, 188–197.
13. Gonzalez, M. C., Toledo, J. D., Tricerri, M. A., and Garda, H. A. (2008) The central type Y amphipathic alpha-helices of apolipoprotein AI are involved in the mobilization of intracellular cholesterol depots. *Arch. Biochem. Biophys. 473*, 34–41.
14. Garda, H. A. (2007) Structure−function relationships in human apolipoprotein A-I: role of a central helix pair. *Future Lipidol. 2*, 95–104.
15. Panagotopulos, S. E., Horace, E. M., Maiorano, J. N., and Davidson, W. S. (2001) Apolipoprotein A-I adopts a belt-like orientation in reconstituted high density lipoproteins. *J. Biol. Chem. 276*, 42965–42970.
16. Panagotopulos, S. E., Witting, S. R., Horace, E. M., Maiorano, J. N., and Davidson, W. S. (2002) Bacterial expression and characterization of mature apolipoprotein A-I. *Protein Expression Purif. 25*, 353–361.
17. Garda, H. A., Arrese, E. L., and Soulages, J. L. (2002) Structure of apolipophorin-III in discoidal lipoproteins: interhelical distances in the lipid bound state and conformational change of ApoLp-III upon binding to lipid. *J. Biol. Chem. 277*, 19773–19782.
18. Runnels, L. W., and Scarlata, S. F. (1995) Theory and application of fluorescence homotransfer to melittin oligomerization. *Biophys. J. 69*, 1569–1583.
19. Vitello, L. B., and Scanu, A. M. (1976) Studies on human serum high density lipoproteins. Self-association of apolipoprotein A-I in aqueous solutions. *J. Biol. Chem. 251*, 1131–1136.
20. Lakowicz, J. R. (1999) Principles of Fluorescence Spectroscopy, 2nd ed., Kluwer Academic/Plenum Publishers, New York, Boston, Dordrecht, London, Moscow.
21. Griep, M. A., and McHenry, C. S. (1990) Dissociation of the DNA polymerase III holoenzyme beta 2 subunits is accompanied by conformational change at distal cysteines 333. *J. Biol. Chem. 265*, 20356–20363.
22. Chattopadhyay, A., and London, E. (1987) Parallax method for direct measurement of membrane penetration depth utilizing fluorescence quenching by spin-labeled phospholipids. *Biochemistry 26*, 39–45.
23. Ladokhin, A. S. (1999) Analysis of protein and peptide penetration into membranes by depth-dependent fluorescence quenching: Theoretical considerations. *Biophys. J. 76*, 946–955.
24. McGuire, K. A., Davidson, W. S., and Jonas, A. (1996) High yield overexpression and characterization of human recombinant proapolipoprotein A-I. *J. Lipid Res. 37*, 1519–1528.
25. Holvoet, P., Zhao, Z., Deridder, E., Dhoest, A., and Collen, D. (1996) Effects of deletion of the carboxyl-terminal domain of apoA-I or of its substitution with helices of apoA-II on *in vitro* and *in vivo* lipoprotein association. *J. Biol. Chem. 271*, 19395–19401.
26. Stone, W. L., and Reynolds, J. A. (1975) The self-association of the apo-Gln-I and apo-Gln-II polypeptides of human high density serum lipoproteins. *J. Biol. Chem. 250*, 8045–8048.
27. Abrams, F. S., and London, E. (1992) Calibration of the parallax fluorescence quenching method for determination of membrane penetration depth: refinement and comparison of quenching by spin-labeled and brominated lipids. *Biochemistry 31*, 5312–5327.
28. Abrams, F. S., and London, E. (1993) Extension of the parallax analysis of membrane penetration depth to the polar region of model membranes: use of fluorescence quenching by a spin-label attached to the phospholipid polar headgroup. *Biochemistry 32*, 10826–10831.
29. Chakrabarti, P, and Chakrabarti, S. (1998) C−H···O hydrogen bond involving proline residues in alpha-helices. *J. Mol. Biol. 284*, 867–873.
30. Kelley, L. A., MacCallum, R. M., and Sternberg, M. J. (2000) Enhanced genome annotation using structural profiles in the program 3D-PSSM. *J. Mol. Biol. 299*, 499–520.
31. Nolde, D. E., Sobol, A. G., Pluzhnikov, K. A., Grishin, E. V., and Arseniev, A. S. (1995) Three-dimensional structure of ectatomin from *Ectatomma tuberculatum* ant venom. *J. Biomol. NMR 5*, 1–13.
32. Pluzhnikov, K., Nosyreva, E., Shevchenko, L., Kokoz, Y., Schmalz, D., Hucho, F., and Grishin, E. (1999) Analysis of ectatomin action on cell membranes. *Eur. J. Biochem. 262*, 501–506.
33. Segrest, J. P., Jones, M. K., Klon, A. E., Sheldahl, C. J., Hellinger, M., De Loof, H., and Harvey, S. C. (1999) A detailed molecular belt model for apolipoprotein A-I in discoidal high density lipoprotein. *J. Biol. Chem. 274*, 31755–31758.
34. Li, H., Lyles, D. S., Thomas, M. J., Pan, W., and Sorci-Thomas, M. G. (2000) Structural determination of lipid-bound ApoA-I using fluorescence resonance energy transfer. *J. Biol. Chem. 275*, 37048–37054.
35. Davidson, W. S., and Hilliard, G. M. (2003) The spatial organization of apolipoprotein A-I on the edge of discoidal high density lipoprotein particles: a mass specrometry study. *J. Biol. Chem. 278*, 27199–27207.
36. Li, L., Chen, J., Mishra, V. K., Kurtz, J. A., Cao, D., Klon, A. E., Harvey, S. C., Anantharamaiah, G. M., and Segrest, J. P. (2004) Double belt structure of discoidal high density lipoproteins: molecular basis for size heterogeneity. *J. Mol. Biol. 343*, 1293–1311.
37. Silva, R. A., Hilliard, G. M., Li, L., Segrest, J. P., and Davidson, W. S. (2005) A mass spectrometric determination of the conformation of dimeric apolipoprotein A-I in discoidal high density lipoproteins. *Biochemistry 44*, 8600–8607.
38. Li, Y., Kijac, A. Z., Sligar, S. G., and Rienstra, C. M. (2006) Structural analysis of nanoscale self-assembled discoidal lipid bilayers by solid-state NMR spectroscopy. *Biophys. J. 91*, 3819–3828.
39. Klon, A. E., Segrest, J. P., and Harvey, S. C. (2002) Molecular dynamics simulations on discoidal HDL particles suggest a mechanism for rotation in the apo A-I belt model. *J. Mol. Biol. 324*, 703–721.
40. Shih, A. Y., Denisov, I. G., Phillips, J. C., Sligar, S. G., and Schulten, K. (2005) Molecular dynamics simulations of discoidal bilayers assembled from truncated human lipoproteins. *Biophys. J. 88*, 548–556.
41. Catte, A., Patterson, J. C., Jones, M. K., Jerome, W. G., Bashtovyy, D., Su, Z., Gu, F., Chen, J., Aliste, M. P., Harvey, S. C., Li, L., Weinstein, G., and Segrest, J. P. (2006) Novel changes in discoidal high density lipoprotein morphology: a molecular dynamics study. *Biophys. J. 90*, 4345–4360.
42. Li, H. H., Lyles, D. S., Pan, W., Alexander, E., Thomas, M. J., and Sorci-Thomas, M. G. (2002) ApoA-I structure on discs and spheres. Variable helix registry and conformational states. *J. Biol. Chem. 277*, 39093–39101.
43. Silva, R. A., Huang, R., Morris, J., Fang, J., Gracheva, E. O., Ren, G., Kontush, A., Jerome, W. G., Rye, K. A., and Davidson, W. S. (2008) Structure of apolipoprotein A-I in spherical high density lipoproteins of different sizes. *Proc. Natl. Acad. Sci. U.S.A. 105*, 12176–12181.
44. Bhat, S., Sorci-Thomas, M. G., Alexander, E. T., Samuel, M. P., and Thomas, M. J. (2005) Intermolecular contact between globular N-terminal fold and C-terminal domain of ApoA-I stabilizes its lipid-bound conformation: studies employing chemical cross-linking and mass spectrometry. *J. Biol. Chem. 280*, 33015–33025.
45. Bhat, S., Sorci-Thomas, M. G., Tuladhar, R., Samuel, M. P., and Thomas, M. J. (2007) Conformational adaptation of apolipoprotein A-I to discretely sized phospholipid complexes. *Biochemistry 46*, 7811–7821.
46. Tricerri, M. A., Behling Agree, A. K., Sanchez, S. A., Bronski, J., and Jonas, A. (2001) Arrangement of apolipoprotein A-I in reconstituted high-density lipoprotein disks: an alternative model based on fluorescence resonance energy transfer experiments. *Biochemistry 40*, 5065–5074.
47. Maiorano, J. N., Jandacek, R. J., Horace, E. M., and Davidson, W. S. (2004) Identification and structural ramifications of a hinge domain in apolipoprotein A-I discoidal high-density lipoproteins of different size. *Biochemistry 43*, 11717–11726.

48. Martin, D. D., Budamagunta, M. S., Ryan, R. O., Voss, J. C., and Oda, M. N. (2006) Apolipoprotein A-I assumes a "looped belt" conformation on reconstituted high density lipoprotein. *J. Biol. Chem. 281*, 20418–20426.
49. Wu, Z., Wagner, M. A., Zheng, L., Parks, J. S., Shy, J. M., 3rd., Smith, J. D., Gogonea, V., and Hazen, S. L. (2007) The refined structure of nascent HDL reveals a key functional domain for particle maturation and dysfunction. *Nat. Struct. Mol. Biol. 14*, 861–868.
50. Shih, A. Y., Sligar, S. G., and Schulten, K. (2009) Maturation of high-density lipoproteins. *J. R. Soc. Interface 6*, 863–871.
51. Toledo, J. D., Tricerri, M. A., Córsico, B., and Garda, H. A. (2000) Cholesterol flux between lipid vesicles and apolipoprotein AI discs of variable size and composition. *Arch. Biochem. Biophys. 380*, 63–70.
52. Tricerri, M. A., Córsico, B., Toledo, J. D., Garda, H. A., and Brenner, R. R. (1998) Conformation of apolipoprotein AI in reconstituted lipoprotein particles and particle-membrane interaction: effect of cholesterol. *Biochim. Biophys. Acta 1391*, 67–78.